

Numerical FE² Study of Chloride Ingress in Unsaturated Recycled Aggregates Concrete

Arthur Fanara^{a,b,*}, Luc Courard^a, Frédéric Collin^a

^a*Urban and Environmental Engineering, University of Liege, Belgium*

^b*FNRS-F.R.I.A, Fonds de la Recherche Scientifique, Belgium*

Abstract

The analysis of the impact of Recycled Concrete Aggregates (RCA) on chloride ingress is of prime importance for the development of Recycled Aggregates Concrete. A coupled chemo-hydraulic multiscale model, using the Finite Element squared (FE²) method, has been developed, validated and calibrated. The constitutive equations using intrinsic parameters derived from laboratory experiments on concrete samples have been established. The findings indicate that the durability of Recycled Aggregates Concrete (RAC) could be comparable to that of Natural Aggregates Concrete (NAC) depending on the mixture quality and environmental conditions. The main difference in durability comes from the rate of diffusion with regards to the mortar paste adherent content.

Keywords: Durability, Finite Element Analysis, Microstructure, Multiscale Modelling, Recycled Aggregates, Transport Properties

1. Introduction

The recycling of Construction and Demolition Waste (C&DW) produces Recycled Concrete Aggregates (RCA), offering a sustainable and local aggregate source. RCA comprises of two phases - original Natural Aggregates (NA) and residual adherent mortar. The latter's quantity depends on the recycling procedure and aggregate dimensions [1, 2, 3]. The

*Corresponding author.

Email addresses: `arthur.fanara@uliege.be` (Arthur Fanara), `luc.courard@uliege.be` (Luc Courard), `f.collin@uliege.be` (Frédéric Collin)

Preprint submitted to Cement and Concrete Research

21st September 2024

residual adherent mortar impairs both the mechanical properties and durability of Recycled Aggregate Concrete (RAC). Studies have demonstrated that incorporating RCA into concrete leads to an elevation in porosity and water absorption, promoting the absorption of water and chloride ions while increasing the overall diffusion of aggressive ions [1, 4, 5, 6]. RCA has been extensively studied for several years, with a specific focus on the impact on the mechanical properties of RAC [7, 8, 9, 10]. This study, however, aims to investigate the durability of reinforced concrete containing RCA, specifically in regards to the effects of chloride attacks. Chloride attacks have been proven to be a significant cause of degradation in coastal areas or when reinforced concrete is exposed to de-icing agents [11, 12]. Chloride ions diffuse through the pore solution and concentrate near the steel rebars, ultimately causing their corrosion. This process is classified as pitting corrosion due to its local nature. It results in a loss of reinforcement section, potentially leading to structural failure [13].

The heterogeneity of concrete is well known: its constituents range from nanometre-sized pores to centimetre-sized aggregates [14]. The addition of Recycled Concrete Aggregates enhances this heterogeneity by increasing the number of different materials present. This is the reason why it is computationally impossible to model the entire microstructure of concrete. One solution is to homogenise its properties over some spatial scale. Multiscale modelling, combined with numerical homogenisation techniques, has been developed to allow homogenisation of the properties at a smaller scale, to be scaled up later, and to keep the computational cost acceptable [15, 16]. Two material scales are therefore used in this approach:

- **Macroscale:** the material is assumed to be homogeneous and the constitutive laws must therefore represent the overall behaviour of the material. Mixture theory is often used to introduce multiple phases (e.g. liquid water and water vapour) percolating through the porous medium [17, 18]. Models based on this single scale have a disadvantage: any change in the microstructure (e.g. a change in constituents) requires a new experimental campaign to update the homogenised properties of the material.

- Mesoscale: the entire material structure is represented in the model, including the heterogeneities (e.g. aggregates). Each constituent has its own constitutive equations and set of properties. A model could be based solely on this scale, which would increase the accuracy of the response, but the computational cost is quite high and is therefore not appropriate for metre-scale engineering structures.

Several homogenisation techniques have been developed in the literature, either analytical [19] or numerical [20]. The homogenisation technique implemented in this model is considered as numerical homogenisation: it is formally called the unit cell method, based on the concept of the Representative Volume Element (RVE) [21, 20]. This RVE represents the mesoscale, the volume that must contain all the required material heterogeneities. The material properties and behaviour at the macroscale are then obtained from the modelling of this RVE [20, 21, 15].

Numerous multiscale numerical tools have been developed in recent years. In civil engineering, where real-scale engineering problems are studied, the continuum approach of the Finite Element Method is highly appropriate for the macroscale. For the microscale, several options are available, which range from Finite Element Methods to Discrete Elements Methods [22]. The former approach is more appropriate when studying couplings, such as chemo-thermo-hydraulic couplings [15], as opposed to the latter, which is better suited for solid mechanics and the intricate behaviour of granular materials, including friction, dilatancy, and anisotropy [22]. Therefore, we have opted to utilise the FE² method, also referred to as FEM-FEM, to develop our model, as the durability of concrete is dependent on the flow of water and gas, amongst other.

A specificity of the FEM at the macroscale is that the material properties and behaviour are only known at the macroscopic integration points, due to the homogenisation of the RVE results [21, 20]. In fact, the integration points of the discretised homogenised macrostructure are bound to a RVE and the finite element computations are performed for each RVE independently, assuming a periodicity of the microstructure near the integration point.

The developed model is a multi-physics FE² model, accurately representing water and gas flow, as well as advection and diffusion of chloride ions within a porous system, such as concrete. In the multiscale approach, appropriate averages over the mesoscale must replace macroscopic phenomenological quantities of interest, including storage terms and flow quantities. The constitutive equations, namely Darcy's and Fick's laws among others, are used at the mesoscale. In addition, homogenisation and localisation equations are employed to derive the macroscopic flows based on the phenomenological quantities of interest at the mesoscale. This process demands a significant space and time scale separation between the mesoscale and macroscale: the diffusion problem must be solved under steady-state conditions at the mesoscale. This hypothesis of steady-state also explains the necessity to perform a numerical homogenisation based on the concept of RVE instead of a direct numerical homogenisation.

The next section of this paper explains in more detail the FE² model developed. First, a mathematical description of a general multiscale model is presented in Section 2.1. Then, in Section 2.2, the constitutive equations implemented for the mesoscale water and gas flows, as well as for the mesoscale chloride ingress, are presented. Finally, Section 2.3 shows the algorithm developed to generate a Representative Volume Element that accurately replicates a 2D slice of concrete.

After presenting the theoretical aspects, the results of several modelling applications are presented in Section 3. The validation of the model under saturated conditions is presented first, followed by validation under unsaturated conditions. An experiment is also reproduced numerically to validate the effects of the RVE. It confirms the ability of our model to replicate the results of any concrete materials through the use of that RVE. Finally, an application based on a real scenario is described, allowing a better understanding of the effects of replacing natural aggregates by recycled aggregates.

Finally, before concluding in Section 5, a sensitivity analysis of the RVE is performed in Section 4.

Throughout this paper, the necessary constitutive properties for the model are obtained through an extensive experimental campaign, which is detailed in Fanara (2023) [23].

2. FE² Model

The numerical double-scale method employed in this paper can be summarised by four iterative steps performed on each Gaussian point of the macroscale mesh until the two scales converge [24]:

1. Localisation: the macroscale boundary conditions are localised at each gauss point and transformed into gradients and mean values (e.g. water and gas pressures, chloride concentration, ...), which are passed on as mesoscale boundary conditions;
2. Resolution of the mesoscale boundary value problem by finite element analysis;
3. Homogenisation: the fluxes obtained at each mesoscale integration point are homogenised to obtain a unique value per macroscale Gauss point;
4. Resolution of the macroscale boundary value problem by finite element analysis.

Theses steps will be elaborated in the following sections.

2.1. Mathematical Description

The multiscale modelling approach couples a subscale and a macroscale. The macroscale component ϕ^M and the subscale component ϕ^s of each scalar field ϕ are added together while the subscale portion defines the fluctuations of the total scalar field [25, 15]:

$$\phi = \phi^M + \phi^s \tag{1}$$

If both components are coupled, then, on the boundaries of the Representative Volume Element, denoted as Γ , the subscale component ϕ^s is considered to be zero, leading to the solution of our model being $\phi = \phi^M$ [16]. However, periodic boundary conditions are used if both fields are uncoupled, allowing the use of a Taylor expansion to establish the macroscale scalar field. Within the macroscale continuum, the expansion can be restricted to its first

114 order using the homogenisation technique's assumption of a linear variation of ϕ^M inside
 115 the RVE:

$$\phi^M(x, \bar{x}) \approx \bar{\phi}(\bar{x}) + \bar{g}(\bar{x}) \times (x - \bar{x}) \quad \forall x \in \Omega \quad (2)$$

116 where \bar{x} represents the centre of the RVE, and \bar{g} denotes a gradient that is defined by:

$$\bar{g}(\bar{x}) = \text{grad } \bar{\phi}(\bar{x}) \quad (3)$$

117 The Taylor expansion is illustrated in Figure 1 for a 1D RVE.

118

119 In the subscale, it is not always certain that the scalar field will exhibit continuity. As a
 120 result, the higher order terms of the Taylor expansion are significant and cannot be ignored.
 121 To account for changes in material properties, a fluctuation field ϕ^f is thus substituted to
 122 the higher order terms [15]:

$$\begin{aligned} \phi(x, \bar{x}) &= \phi^M(x, \bar{x}) + \phi^f(x) \\ &= \bar{\phi}(\bar{x}) + \bar{g}(\bar{x}) \times (x - \bar{x}) + \phi^f(x) \end{aligned} \quad (4)$$

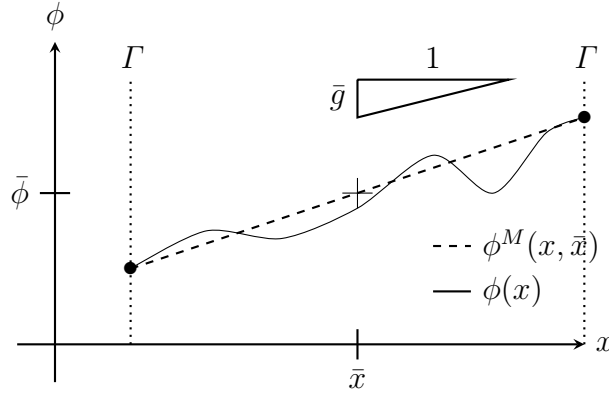


Figure 1: Illustration of the Taylor expansion limited to its first order, for a 1D RVE domain Ω (modified from [16]).

123 However, it is essential that both the macroscale and the subscale components of the
 124 scalar field are identical at all points on the macroscale. Hence:

$$\bar{g}(\bar{x}) \times (x - \bar{x}) + \phi^f(x) \ll \bar{\phi}(\bar{x}) \quad (5)$$

where the concept of separation of scales arises. It is required that the subscale's characteristic length (l_c^s) is negligible compared to the macroscopic field's characteristic fluctuation length (L_c^M) [26, 15].

$$l_c^s \ll L_c^M \quad (6)$$

First-order homogenisation techniques require the verification of this assumption. If this condition is not verified, the local macroscale gradients cannot determine the boundary conditions of the subscale.

The transition from the subscale back to the macroscale, namely numerical homogenisation, necessitates the transfer of the flux. Under stationary conditions, the mass balance equation writes:

$$\nabla J = 0 \text{ in } \Omega \quad (7)$$

where J is the homogenised flux and Ω is the domain occupied by the RVE, where the material heterogeneities are embedded.

The scalar field division and first-order homogenisation thus enable the determination of the volume average \bar{J} of the flux within the RVE:

$$\bar{J} = \frac{1}{|\Omega|} \int_{\Omega} J(x) d\Omega \quad (8)$$

that is the macroscale flux.

2.2. Constitutive Equations

The multiscale model has been created to cater for both saturated and unsaturated scenarios. At the macroscale, three degrees of freedom, i.e. water pressure, gas pressure and chloride concentration, are defined and used as boundary conditions. Afterwards, gradient and mean values of aforementioned degrees of freedom are conveyed to the RVE for every Gauss point. Based on these localised boundary conditions, a value of the water pressure, gas pressure and chloride concentration is assigned to each integration point of the subscale. The boundary value problem at the subscale can then be resolved.

2.2.1. Mesoscale Water Flows

The mass balance equation of liquid water inside the porous matrix of concrete, in a fixed and underformable system, under the hypothesis of steady-state, is:

$$\frac{\partial}{\partial x_i} (\rho_w v_i^w) = 0 \quad (9)$$

where ρ_w is the water density [kg/m³] and v_i^w is the fluid flow rate per unit area [m/s].

The first factor of the Equation 9, that is the water density, varies with the mean water pressure:

$$\rho_w = \rho_{w0} \times \left(1 + \frac{P_{w,average} - P_{w0}}{\chi_w} \right) \quad (10)$$

where ρ_{w0} is the initial density of liquid water, $P_{w,average}$ [Pa] is the mean pressure at the macroscale integration point and P_{w0} [Pa] is the initial pressure inside the porous structure (pressure at which ρ_{w0} was calculated). This relation is also dependent on the fluid compressibility, noted χ_w [Pa⁻¹] (at 20°C, $1/\chi_w = 5 \cdot 10^{-10}$ Pa⁻¹). The water density may also vary depending on the ionic concentration of chlorides, but it has been neglected at this stage, its influence being deemed less important than the one of the water pressure.

The second factor of the Equation 9 expresses the liquid water flow. The Darcy's law is used to describe this movement of liquid water inside the porous medium. Under the hypothesis of a homogeneously permeable medium, and in the absence of gravitational forces (therefore the equations are the same along all directions), the fluid flux and the gradient of water pressure are directly proportional:

$$v_i^w = - \frac{k_{int} k_{rel,w}}{\mu_w} \frac{\partial P_w}{\partial x_i} \quad (11)$$

where k_{int} [m²] is the intrinsic permeability of the porous matrix and $k_{rel,w}$ [-] is the water relative permeability, μ_w [Pa.s] is the dynamic viscosity of water and $(\partial P_w)/(\partial x_i)$ is the gradient of water pressure.

171 The relative permeability $k_{rel,w}$ is dependent on the degree of saturation of the porous
 172 matrix. It is theoretically equal to 0 in perfectly dry conditions, or equal to 1 in saturated
 173 conditions. The empirical equation used to express this relative permeability is the one of
 174 Van Genuchten [27]:

$$k_{rel,w} = \sqrt{S_{r,w}} \times \left(1 - \left(1 - S_{r,w}^{1/m_{VG}}\right)^{m_{VG}}\right)^2 \quad (12)$$

175 where $S_{r,w}$ [-] is the degree of saturation in liquid water of the porous medium and m_{VG}
 176 [-] is a model parameter associated to the curvature of the water retention curve [28]. The
 177 degree of saturation is also obtained by an empirical equation from Van Genuchten [27]:

$$S_{r,w} = S_{res} + (S_{sat} - S_{res}) \left(1 + \left(\frac{s}{\alpha_{VG}}\right)^{n_{VG}}\right)^{-m_{VG}} \quad (13)$$

178 where n_{VG} [-] is another model parameter related to the rate of desaturation of the soil
 179 (equal to $1/(1 - m_{VG})$) and α_{VG} [Pa] is the air-entry pressure. Two other parameters, S_{res}
 180 [-] and S_{sat} [-] are, respectively, the residual saturation of the medium and the maximum
 181 saturation of the medium. Finally, the suction s [Pa] is the matrix suction defined as the
 182 difference between the gas pressure and the liquid water pressure:

$$s = p_g - p_w \quad (14)$$

183 2.2.2. Mesoscale Gas Flows

184 The mass balance equation of gaseous air inside the porous matrix of concrete, under
 185 the same hypothesis as for the water, is:

$$\frac{\partial}{\partial x_i} (\rho_g v_i^g) = 0 \quad (15)$$

186 where ρ_g is the air density [kg/m³] and v_i^g is the gas flow rate per unit area [m/s].
 187

188 The first term of the Equation 15, that is the gas density, varies with the mean gas
 189 pressure of the matrix:

$$\rho_g = \rho_{g0} \times \left(\frac{P_{g,average}}{P_{g0}}\right) \quad (16)$$

where ρ_{g0} is the initial density of gaseous air, $P_{g,average}$ [Pa] is the mean gas pressure at the macroscale integration point, and P_{g0} [Pa] is the initial gas pressure inside the porous structure (pressure at which ρ_{g0} was computed).

The second factor of the Equation 15 expresses the gaseous air flow. The Darcy's law is also used to describe this movement of gaseous air inside the porous medium. Under the same assumptions as for the liquid water, the gas flux writes:

$$v_i^g = -\frac{k_{int} k_{rel,g}}{\mu_g} \frac{\partial P_g}{\partial x_i} \quad (17)$$

where k_{int} [m²] is the intrinsic permeability of the porous matrix and $k_{rel,g}$ [-] is the gas relative permeability. The term μ_g [Pa.s] is the dynamic viscosity of the gas and $(\partial P_g)/(\partial x_i)$ is the gradient of pressure.

The relative permeability of gas is computed with the same model as for the relative permeability of water based on the principle that the porous matrix must be completely filled with water and gas, therefore the addition of the degree of saturation of liquid water and the one of gaseous air must be equal to one [27]:

$$k_{rel,g} = \sqrt{1 - S_{r,w}} \times (1 - S_{r,w}^{1/m_{VG}})^{2 m_{VG}} \quad (18)$$

A component of dissolved air could be taken into account in the model, as well as a component of water vapour [29]. However, at this stage in the development of the model, these two species have not been implemented. The errors introduced by not accounting for these components may be neglected as the water vapour is nearly absent at the temperatures studied in our model (around 20°C) [29], and the gas pressure is fixed throughout our system, the unsaturated conditions being controlled through the evolution of the water pressure.

2.2.3. Mesoscale Chloride Ingress

The balance equation of the chloride ions is:

$$\frac{\partial}{\partial x_i}(v_i^c) = 0 \quad (19)$$

where v_i^c [m/s] is the chlorides flow rate per unit area.

The chlorides flow rate can be caused by an addition of three phenomena: advection, dispersion and diffusion [30, 31, 32, 33, 34, 35]. The first one is a movement of the chlorides inside water due to water flows. The second one is due to the irregularity of the porous system, causing a local variation of the concentration. The last one is due to a gradient of concentration inside the fluid itself. One can therefore write:

$$\begin{aligned} v_i^c &= v_i^{\text{advection}} + v_i^{\text{diffusion+dispersion}} \\ &= C_M v_i^w - D \frac{\partial C_m}{\partial x_i} \end{aligned} \quad (20)$$

where C_M [-] and C_m [-] are, respectively, the concentration in chloride ions at the macroscale and mesoscale integration points, v_i^w [m/s] is the water velocity obtained with Darcy's law and D [m²/s] is the diffusion and dispersion coefficient, obtained experimentally.

2.2.4. Macroscale Mass Balance Equations

The mass balance equations for the multiple species (water, gas and chloride ions) occupying the pore space of the macroscale are the following, respectively:

$$\frac{\partial}{\partial x_i} (\rho_w \times v_{i,\text{homogenised}}^w) + \frac{\partial S_w}{\partial t} = 0 \quad (21)$$

$$\frac{\partial}{\partial x_i} (\rho_g \times v_{i,\text{homogenised}}^g) + \frac{\partial S_g}{\partial t} = 0 \quad (22)$$

$$\frac{\partial}{\partial x_i} (C_M \times v_{i,\text{homogenised}}^w + v_{i,\text{homogenised}}^c) + \frac{\partial S_c}{\partial t} = 0 \quad (23)$$

where one recognizes the spatial variation of the flux and the temporal variation of the storage, for each species. The homogenised water, gas and chloride ions fluxes are obtained through the spatial homogenisation of the flux computed at the mesoscale, proportionally to the relative surface of the RVE, as explained hereabove. The storage terms, on the other hand, are computed by calculating the total mass of each species over the RVE, at each given time. For the chloride ions, the coupling between the water flows and the chloride advection is expressed at the macroscale, by multiplying the homogenised water flows and the mean macroscale concentration in chloride ions.

2.2.5. Homogenised Macroscale Response

The constitutive equations explained above for the mesoscale solution are solved following a fully coupled finite element scheme, with analytical stiffness matrices. The mesoscale fluxes are thus obtained as a solution of the boundary value problem solved. They are then homogenised numerically: the fluxes of each mesoscale integration point are summed proportionally to their relative area. The homogenised flow, after being transmitted to the macroscale point of integration, is utilised to calculate the macroscale internal fluxes. The problem is subsequently solved through the use of a finite element scheme.

The elementary stiffness matrix of the macroscale problem is obtained through perturbation, unlike that of the mesoscale [36]. The gradients and mean values of water and gas pressure, as well as chloride concentration, are perturbed in sequence, after which the stiffness matrix is computed for the macroscale based on these perturbations:

$$K_{i,j} = \frac{\text{Flux}_{i,\text{perturbated}} - \text{Flux}_{i,\text{original}}}{\text{Perturbation}_j} \quad (24)$$

The method is time-consuming since it necessitates solving mesoscale calculations ten times. Nevertheless, it is imperative to obtain a consistent tangent operator as the problem is highly non-linear.

2.3. Representative Volume Element

The mesoscale, the key element of the multiscale formulation, is modelled by a representative volume element (RVE). For this research, where our focus is on aggregate substitution, this RVE must represent a 2D slice of concrete whose scale is similar to the samples used for the experimental campaign, that is pluri-centimetre samples. This means that the RVE is made up of a homogenised mortar paste (with homogenised properties) filled with impervious aggregates and, for recycled concrete aggregates, an adherent homogenised mortar paste [37]. Other studies would also place the ITZ between the aggregates and the mortar paste, and between the aggregates and the adherent mortar for RCA [38, 33, 39, 4, 40]. However, our model is based on properties that can be determined experimentally and the nature of

the ITZ makes it impossible to characterise this phase specifically. It was therefore decided to omit the ITZ rather than add uncertainties to the model.

The parameters in the mesoscale equations are inherent material properties. These properties are only related to a single phase, within either the adherent mortar or the new mortar matrix, depending on the location of the integration point at the mesoscale. At the macroscale, however, the material is considered as a composite represented by a single homogenised phase. Thus all its properties are averaged effective properties.

The mesoscale is defined with a characteristic length of the order of a centimetre, while the macroscale has a characteristic length of the order of a metre and above, to respect the principle of separation of scales.

Multiple ways of generating an RVE are available, including image analysis and algorithm development [41, 16]. The former method enables the creation of a relatively precise concrete slice based on an image, whereas the latter relies purely on intrinsic features of the concrete mixture. For this study, an algorithm designed specifically for our model and based on that of Nilenius (2014) [25] was employed to generate the RVE.

The algorithm is presented in Figure 2. The process necessitates several intrinsic properties of the concrete mix, including the Particle Size Distribution (PSD) of the aggregates, the Surface Fraction (SF) of aggregates within the mix, and their Aspect Ratio (AR). These are applied to generate a random 2D slice of concrete, which accurately represents the concrete produced in the laboratory.

The first step in the algorithm is to compute the area required for each interval of the particle size distribution. Based on the RVE size and the surface fraction of aggregates (that is, under the strong hypothesis that the surface fraction is equivalent to the volume fraction, the volume of aggregate for one cubic metre of concrete), the required aggregate surface area can be determined. According to the particle size distribution, the total surface of aggregate is then distributed between the diameter intervals. Finally, the RVE is filled with aggregates from the largest diameter interval to the smallest. When an aggregate cannot be

288 placed without exceeding the required area, then the interval is considered complete and a
289 smaller one is filled.

290 The generation of the aggregate follows a random pattern. First, a random size is taken
291 from the current diameter interval and used to generate an elliptical aggregate that meets
292 the required aspect ratio. Next, the ellipse is degenerated into an octagon and all vertices
293 are shifted slightly to emphasise the random aspect of the aggregate. Finally, this aggregate
294 is randomly placed inside the RVE. To ensure that the aggregates do not make contact with
295 each other, a non-intersection criterion is evaluated to confirm their respective positions.
296 If there is an intersection with aggregates already placed, the latest one is deleted and a
297 new aggregate is created. The rationale behind this is that the new aggregate may intersect
298 several others. It is therefore more efficient to delete the new one than the ones already
299 placed.

300 Once an aggregate is placed into the RVE, the surface fraction is updated, and we may move
301 on to the final step, provided that the concrete slice created comes from Recycled Aggregate
302 Concrete. This step involves modelling recycled concrete aggregate (RCA) as a natural
303 aggregate with a surrounding layer of adherent mortar. The surface area of the mortar layer
304 is equal to a specified percentage of the RCA. After completing the entire RVE, it is meshed
305 with the use of a different software from the University of Liege, namely gmsh [42]. Figure
306 3 presents an example of a generated and meshed RVE, which displays a blue mesh with
307 properties of the homogenised mortar, an orange mesh with properties of the homogenised
308 adherent mortar, and unmeshed, white impervious aggregates.

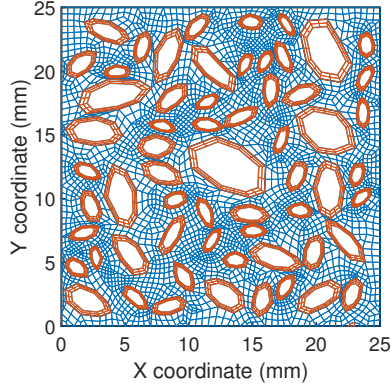


Figure 3: Example of a RVE representing a concrete slice with recycled concrete aggregates. It was generated with the algorithm developed and meshed with the software gmsh [42]. The new mortar is meshed in blue, the adherent mortar of the RCA is meshed in orange and the natural aggregates inside the RCA, considered impervious, are unmeshed.

This algorithm, whilst robust, has several drawbacks based on the underlying assumptions including:

- The surface fraction corresponds to the volume fraction of aggregate. However, this is only partially correct due to the non-homogeneous distribution of aggregates in concrete. Consequently, not all sections possess an identical surface fraction.
- The distribution of particle sizes in the aggregates differs from that in a concrete slice. The aggregates are non-spherical, meaning their size and shape can vary depending on their orientation.

One way to reduce inaccuracies resulting from these hypotheses is through reverse modelling and verifying that the Representative Volume Element (RVE) accurately replicates experiments conducted in the laboratory, for instance. It is shown later in this paper, in Section 3.3.

3. Results

3.1. Validation of the Model under Saturated Conditions

After constructing a model, the initial stage is the validation. Whenever achievable, the validation process must be analytical, but when necessary, it can be numerical by using other

previously validated models. Analytical solutions can be retrieved from existing literature for saturated conditions, and this study utilises the solution from Biver (1993) [35]. For a one-dimensional semi-infinite medium, the solution for the diffusion and advection of chloride ions can be expressed by [35, 43]:

$$C(x, t) = \frac{C_0}{2} \exp\left(\frac{ux}{2D}\right) \times \left[\exp\left(-x\frac{u}{2D}\right) \operatorname{erfc}\left(\frac{x}{2\sqrt{Dt}} - \sqrt{\frac{u^2t}{4D}}\right) + \exp\left(x\frac{u}{2D}\right) \operatorname{erfc}\left(\frac{x}{2\sqrt{Dt}} + \sqrt{\frac{u^2t}{4D}}\right) \right] \quad (25)$$

where the limit state condition C_0 [mg/ml], the fluid flow u [m/s] and the diffusion coefficient D [m²/s] can be observed. This equation evolves both in time (t [s]) and in space (x [m]). In the absence of fluid flow, it is equivalent to Fick's second law solution. Fluid flows may be calculated using Darcy's law:

$$u = -\frac{k_{int}}{\mu_w} \frac{\partial P_w}{\partial x} \quad (26)$$

The results of the analytical solution, represented by Equation 25, are shown in Figure 4. The parameters used in both the analytical validation and the developed multiscale model are given in Table 1. The RVE of the multiscale model to be compared with an analytical solution must be completely homogenised with a single phase. It can be seen that the analytical results (dots), are in perfect agreement with the numerical results (straight lines), thus validating the multiscale model for saturated conditions.

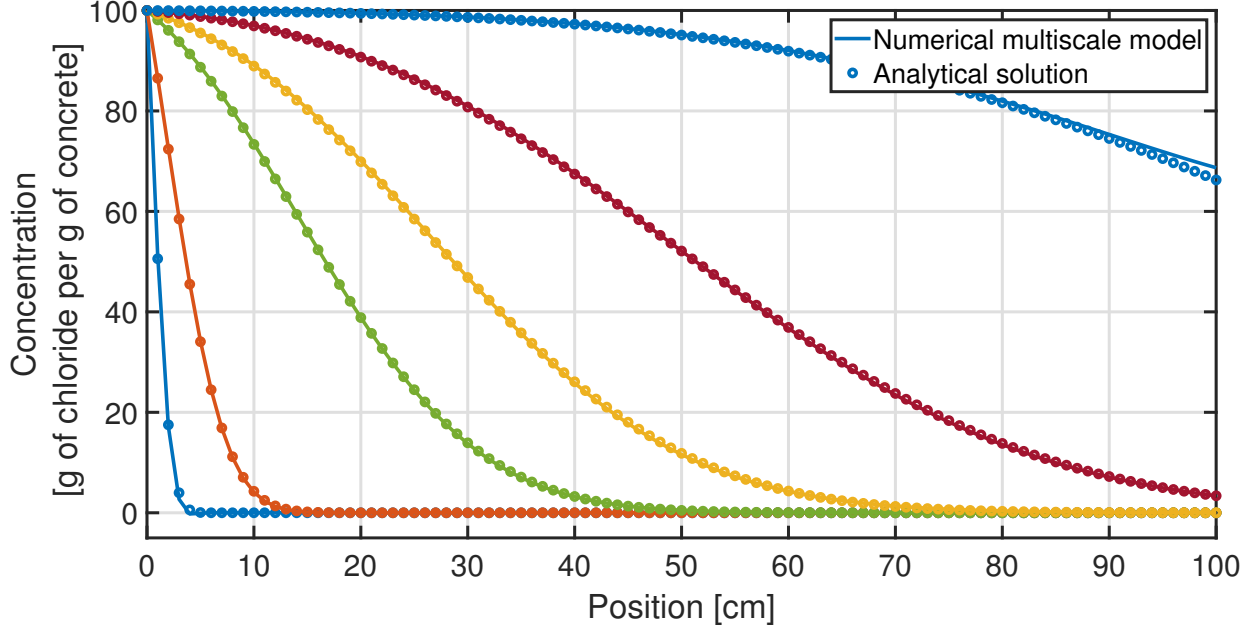


Figure 4: Analytical validation of the multiscale model for the diffusion and advection of chloride ions under saturated conditions. Each color represents a different simulation time.

C_0 [mg/ml]	D [m ² /s]	u [m/s]	k_{int} [m ²]	μ_w [kg/m.s]	$\partial P_w / \partial x$ [Pa/m]
100	1E-12	4E-13	1E-19	1E-3	4E3

Table 1: Properties of the material used to analytically validate the multiscale model under saturated conditions.

3.2. Validation of the Model under Unsaturated Conditions

Under unsaturated conditions, the model exhibits significant non-linearity, making analytical validation difficult. Consequently, numerical validation was preferred, utilising established single scale models developed at the University of Liège [35, 29]. The combination of WAVAT and ADVEC laws, which were developed using the LAGAMINE software employed for this multiscale model, enables the simulation of advection and diffusion of any pollutants within an unsaturated porous medium. A homogeneous RVE was necessary for comparing the responses. Initially, the medium has zero chloride concentration, and the gas and water pressures throughout are equivalent to the atmospheric pressure. Then, the boundary

conditions are applied on the left border as shown in Figure 5. The water pressure varies cyclically from -124.39MPa to -6.96MPa, while the concentration of chloride ions rises to 100 g of chloride per g of concrete and remains constant thereafter.

The outcomes of the numerical validation are illustrated in Figures 6 and 7, denoting the chloride concentration and water pressure, respectively. The time and boundary conditions displayed by markers in Figure 5 refer to the responses of Figures 6 and 7.

The outcomes of the recently developed multiscale model are shown with dashed lines and triangle markers, while the outcomes of the already validated single scale model are illustrated with solid lines. It is evident that there is a satisfactory match between the two responses for both the water pressure and chloride concentration, indicating the validation of our model for chloride ion advection and diffusion within an unsaturated porous medium.

3.3. Replication of Experimental Results

The validated model was then compared with experimental results to evaluate its ability to accurately portray reality. The experiment on chloride diffusion under transient state conditions is an ideal case for this application [23]. The experiment tested three compositions: an equivalent mortar (E-M), a concrete made from NA (NAC) and another from RCA (RAC). Several additional experiments were conducted to determine the necessary intrinsic parameters of the materials, including intrinsic water permeability, porosity, and diffusion coefficient. The experimental intrinsic properties incorporated into the model are indicated in Table 2.

The macroscopic mesh that depicts the experimental sample (that is a cylinder 5cm high and with a diameter of 10cm), is shown in Figure 9. The boundary conditions are enforced at the left of the mesh in Figure 9, which allows for chloride ions to leach into the porous structure in an unidirectional manner. The water pressure remains constant at atmospheric pressure to maintain a saturation degree of 1. Additionally, the chloride concentration matches the surface concentration (C_s) value of the corresponding concrete, which is listed in Table 2. This surface concentration depends on the chloride content of the solution, as well as on the

porosity and density of the material, as depicted in this equation:

$$C_s[\%] = C_{\text{solution}} [\text{g/L Cl}^-] \frac{n [\% \text{ volume}]}{\rho_d [\text{kg/m}^3]} \quad (27)$$

The mesoscopic meshes provided in Figure 8 depict sections of either NAC or RAC.

The results of the experimental validation can be viewed in Figures 10 and 11. The data points in black represent the experimental results obtained over 15, 29 and 91 days of diffusion [23]. We carried out various comparisons, starting with an RVE that was homogeneous and had properties similar to those of the NAC or RAC obtained during the experimental campaign. Figures 10 and 11 show the results in solid lines. These lines represent the best fit of our model to the experimental results, owing to the time variation of the diffusion coefficient expressed experimentally, whereas our model requires a single value of the diffusion coefficient. Nonetheless, these findings are favourable when compared to the experimental results, particularly the 29-day results which yielded the diffusion coefficient used numerically. Furthermore, that diffusion coefficient was obtained through the fitting of Fick's law, the same law introduced into our model, confirming that it would not be possible to get a better fit of the experimental results.

Property	E-M	NAC	RAC
Intrinsic Permeability [m ²]	3.87E-18	1.73E-19	2.58E-19
Porosity [% Volume]	22.83	14.16	20.50
Diffusion Coefficient [m ² /s]	1.43E-11	1.41E-11	1.65E-11
C_s [%]	1.45	0.78	1.27

Table 2: Intrinsic properties of the E-M, NAC and RAC obtained experimentally and implemented in the constitutive laws of the multiscale model.

The RVE depicted in Figure 8 was subsequently utilised, requiring the input of equivalent mortar paste (E-M) material properties as only the mortar is meshed in the RVE, with the aggregates being impervious. The resultant response, represented by a dashed line, is less precise than anticipated. However, accurate results are obtained by increasing the diffusive

properties of the mortar paste by 30%. This is due to the two-dimensional aspect of our model in comparison to a 3D experiment. Such findings are in line with previous studies, which state that the diffusion can increase up to 40% when the model is in 3D instead of 2D [25].

For the RAC, it is possible that the properties of the adherent mortar differ from those of the plain mortar paste. However, obtaining these properties experimentally is impossible, except through the use of reverse modeling. Initially, all phases of the RAC RVE utilise the properties of the E-M composition, just like the NAC. The RVE is indeed what distinguishes the two concrete types. To enable a comparison between the NAC and RAC, the parameters have also been increased by 30%. The outcomes are presented in dotted lines and represent a fairly accurate reflection of the experimental results.

3.4. Application on a Real Life Scenario

An application has been developed, based on a real scenario, to study the difference in durability between a concrete made from natural aggregates and one made from recycled concrete aggregates. The most critical environment in terms of chloride attack is the marine environment. It was therefore decided to study a reinforced concrete lock wall in direct contact with salt water. This wall is in contact with water on both sides: it is therefore divided in two in the model, under the hypothesis of a symmetrical response.

The lock wall is shown in Figure 12. It is 50cm wide, 4m high out of the water, and 2m deep under water. Of course, a real lock wall would be deeper than this, but it was verified previously that the response is constant under 2m of water, as the water pressure remains hydrostatic (see Figure 13) and the chloride ions only penetrate the concrete through diffusion. As no further information may be deduced from that zone, it has been cropped to reduce the time needed to run the simulation. As one can see, a transition zone is defined between the hydrostatic and atmospheric conditions to smooth the gradient of the water pressure applied to the wall.

The environmental conditions were those of the study conducted by Zuquan et al. [44], and are shown in Table 4. They are applied mensually, with a linear interpolation in between

two months. The chloride concentration in water was chosen to be equal to 17g/L, or approximately 2% of the water density [44]. The chloride content was converted into a surface concentration using the subsequent equation:

$$C_s[\%] = 17 \text{ [g/L Cl}^-] \frac{n \text{ [\% volume]}}{\rho_d \text{ [kg/m}^3]} \quad (28)$$

resulting in a surface concentration of 0.11% for the NAC and 0.17% for the RAC. The chloride concentration in the air was assumed to be 0%. In an ideal numerical simulation, the tides and water droplets should be taken into account. However, due to the time consuming nature of such simulations, this was neglected here.

Property	NAC	RAC
Intrinsic Permeability [m ²]	5.02E-18	5.02E-18
Porosity [% Volume]	29.68	29.68
Diffusion Coefficient [m ² /s]	1.86E-11	1.86E-11
n_{VG} [-]	1.53	1.48
α_{VG} [MPa]	13.83	10.43

Table 3: Intrinsic properties of the NAC and RAC used in the application.

Month	RH [%]	T [K]	P_w [MPa]
Jan.	62.5	273.4	-59.3
Feb.	63.9	275.4	-56.9
Mar.	65.3	279.3	-54.9
Apr.	69.5	287.6	-47.7
May	72.5	290.1	-43.0
Jun.	81.9	293.9	-27.0
Jul.	86.1	297.9	-20.5
Aug.	81.4	298.8	-28.3
Sep.	69.3	295.4	-50.0
Oct.	65.2	289.6	-57.1
Nov.	66.3	282.2	-53.5
Dec.	63.9	276.0	-57.0

Table 4: Environmental conditions (temperature and relative humidity) applied to the pier, and the corresponding water pressure.

For this application, two RVEs were used: one representing the NAC and the other the RAC. Therefore, the properties of the E-M were used for both compositions, increased by 30% as demonstrated in Section 3.3. However, the water retention curve is defined as a macroscale parameter in the model and was therefore defined based on the experimental results of the NAC and RAC, respectively [23]. The parameters used in the model, for both RVE, are provided in Table 3.

The simulation runs for 5 years, before comparing the response of both types of concrete. Figure 13 presents the results for water pressure. The pressure inside the NAC is lower than that inside the RAC. This result implies that the NAC had a more substantial moisture exchange with its surroundings since the water pressure at the boundary is closer to the one applied as boundary conditions. The water saturation degree in Figure 14 confirms that it is lower in the NAC compared to the RAC.

442 These findings contradict expectations that RAC would have higher rates of water and chlor-
443 ide exchange with its environment compared to NAC, as suggested by previous experimental
444 results [23]. However, RAC has a tendency to desaturate more rapidly than NAC, as evid-
445 enced by its water retention curve. Consequently, the decrease in relative permeability due
446 to desaturation may slow down the exchange rates between the core of the concrete and
447 its environment. This is illustrated in Figure 15, where it can be observed that the water
448 permeability of the concrete, which is the product of the intrinsic and relative permeabilit-
449 ies, is lower for RAC than for NAC when the water pressure drops. Additionally, studying
450 the chloride concentration (expressed as a percentage of the binder mass) in both concretes
451 serves as an excellent indicator of the effects of unsaturated conditions. The chloride con-
452 centration of RAC surpasses that of NAC in unsaturated conditions, but it appears to seep
453 more deeply into NAC, as demonstrated in Figure 16. It is noteworthy that RAC also has
454 a higher chloride content than NAC at the bottom of the mesh where both concretes are
455 fully saturated. This can be explained by the fact that RAC is more diffusive. However,
456 around the transition zone from hydrostatic to atmospheric conditions (at a height of 2m),
457 the saturation degree of water reduces, and the phenomenon described above begins. Con-
458 sequently, the NAC exhibits a chloride ion penetration front that is more advanced than
459 that of the RAC.

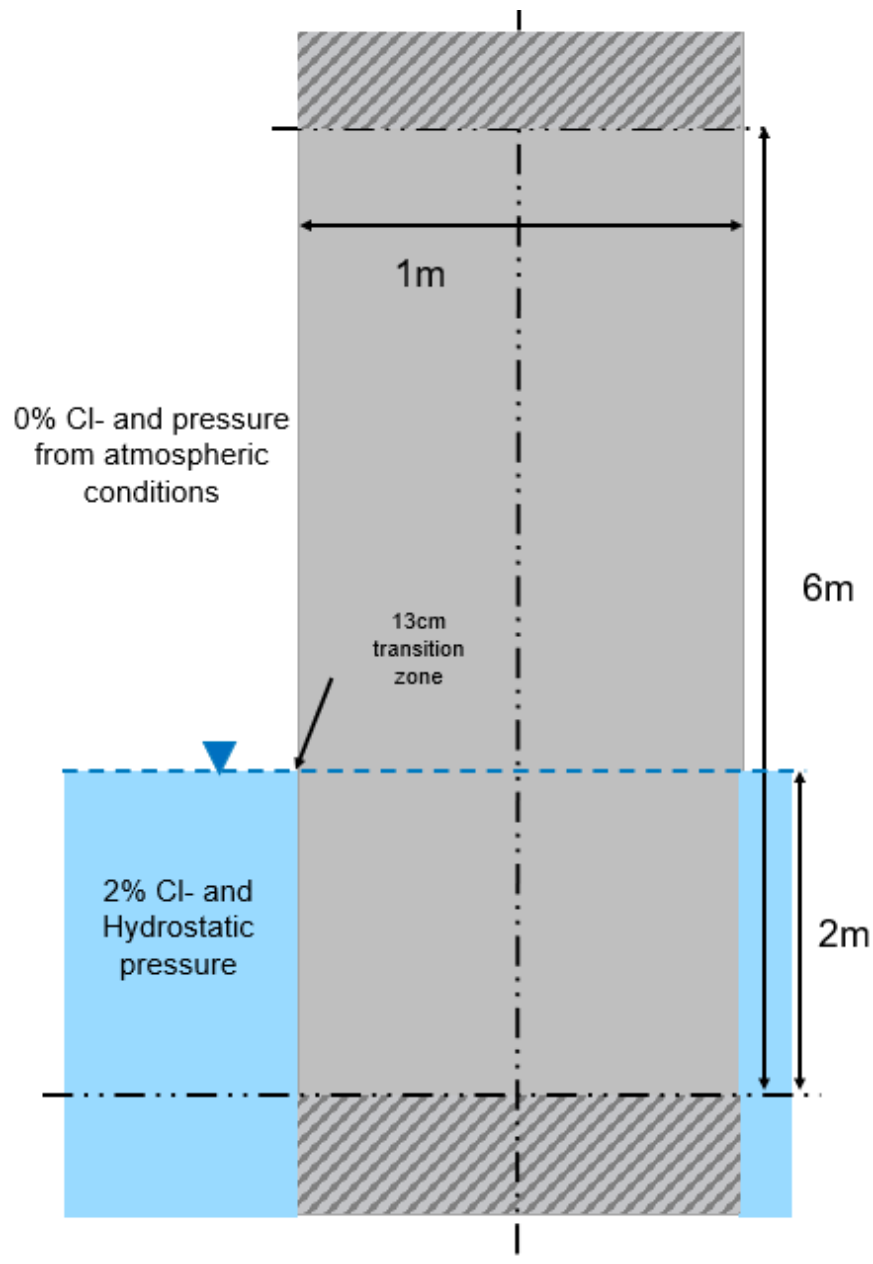


Figure 12: Representation of the lock wall studied in the application of our model. Under symmetric conditions, only half its width is modelled.

4. Discussion

4.1. Sensitivity Analysis of the RVE

Various parameters of the Representative Volume Element undoubtedly affect the outcomes. A sensitivity analysis is, therefore, beneficial in reducing the risk of an incorrect response caused by an inappropriate RVE. Parameters requiring investigation are the RVE's dimensions, the quantity of mortar attached to the Recycled Concrete Aggregates and the characteristics of that specific phase.

4.1.1. Influence of the size of the RVE

The Representative Volume Element (RVE) is a 2D concrete slice with a specific Particle Size Distribution (PSD). To generate the RVE, aggregates must be randomly packed into a designated space to achieve the desired PSD. Smaller RVEs are more challenging to fill, leading to an incomplete PSD and a smaller percentage of impervious aggregates, resulting in a larger diffusive surface area. Figure 17 illustrates that phenomenon for various RVEs displaying diverse sizes for both NAC and RAC. The PSD incorporated in the generation algorithm is also demonstrated. It can be inferred that the PSD created approximates better the theoretical one as the size of the RVE increases.

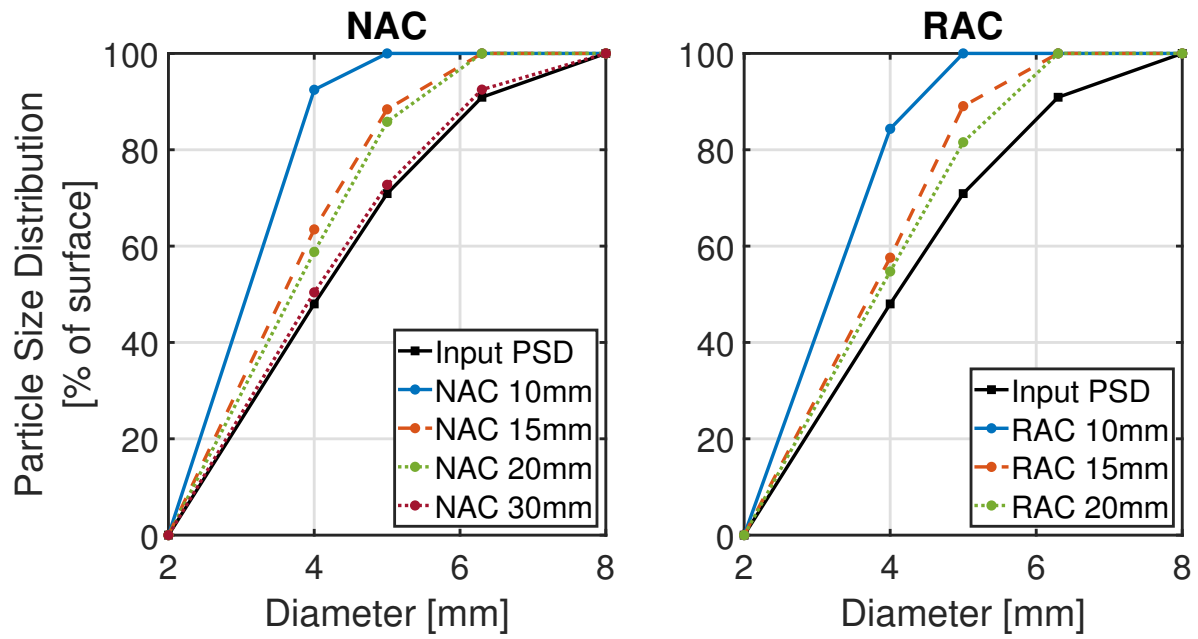


Figure 17: Influence of the RVE Size on the Particle Size Distribution obtained numerically. The results on the left depict a RVE with natural aggregates, while the ones on the right represent a RVE with recycled concrete aggregates.

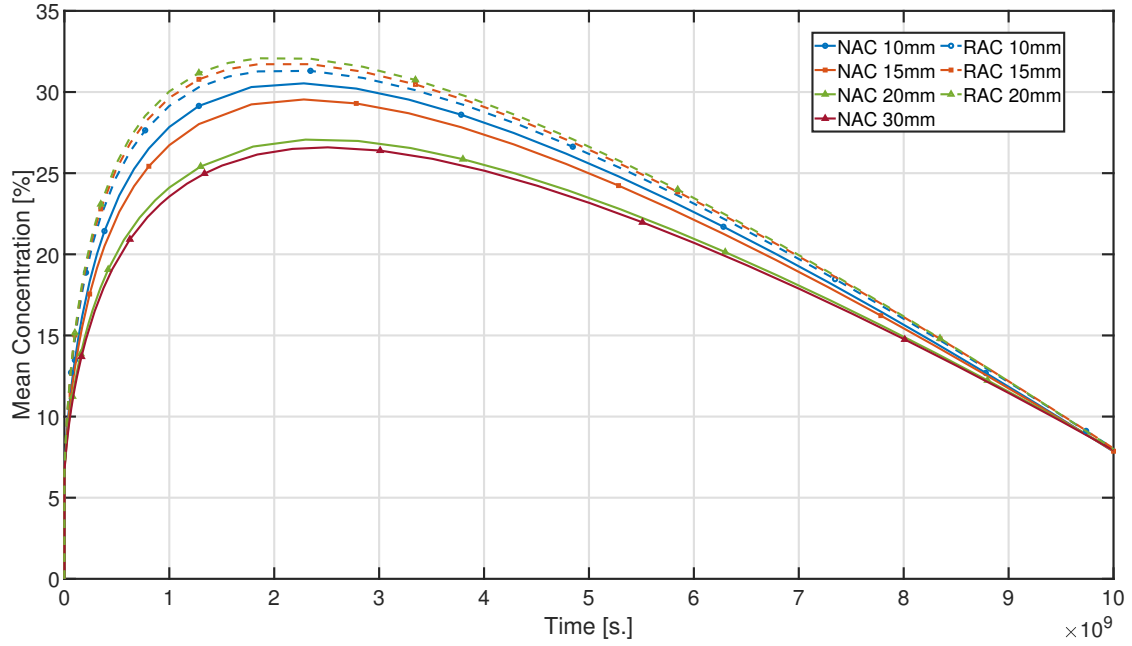


Figure 18: Influence of the RVE Size on a diffusion simulation on NAC and RAC RVEs. The results are expressed in terms of mean chloride concentration throughout the whole mesh as a function of elapsed time.

The various RVEs were used in a straightforward diffusion simulation in fully saturated conditions. Figure 18 illustrates the results, where the vertical axis indicates the mean chloride concentration value of the entire macroscopic sample. A RVE of 30mm size for the RAC has not been tested, in opposition to the NAC, as it would take a very long time to compute and the results are already converged for 20mm. Two relevant observations can be made:

1. Firstly, the RAC exhibits a greater mean concentration than the NAC throughout, due to its higher percentage of diffusive surface area (with equal diffusive properties in both mortar phases). For example, for the RVE with a size of 20mm, the NAC has 67% of diffusive surface area whereas the RAC has 82% of diffusive surface area, for a mean chloride content (over space and time) of 9.9% and 11.4%, respectively;
2. The RAC appears to be less reliant on the size of the RVE in comparison to the NAC. This may be attributed to the larger proportion of diffusive surface in the RAC.

The RVE's minimum size should be 20mm based on these findings. Indeed, the average chloride concentration appears to have converged at this size, as depicted in Figure 18. Nonetheless, larger RVEs require longer computation times, necessitating a compromise between outcome accuracy and simulation costs. Furthermore, note that the simulations with a RVE representing RAC are more intensive than the one representing NAC as there are much more elements in those RVE, due to the meshing of the adherent mortar.

4.1.2. Influence of the quantity and properties of adherent mortar

Another important aspect of the Representative Volume Element is the type of concrete it is intended to represent. When equivalent properties are considered, using one type of concrete over another may impact the results. As shown in Figures 19 to 21, an RVE created from NA (or RCA, or RCA with 20% more adherent mortar) serves as an example.

A one-dimensional problem of chloride diffusion and convection in saturated conditions is then analysed. The water pressure is initially equal to the atmospheric pressure and there are no chloride ions present in the sample. Following this, boundary conditions are implemented on the macroscale mesh's left border, according to Figure 22.

The findings are presented in Figure 23. Firstly, the RAC, which has increased diffusive surface due to recycled aggregates, exhibits higher concentration in chloride ions throughout the experiment compared to NAC, regardless of properties being equal for all phases. That is logical as chloride ions only leach into the porous structure of concrete, the aggregates being impervious. Therefore, the greater the quantity of mortar, the greater the ingress of chloride ions.

Secondly, increasing the amount of adherent mortar in recycled aggregates by 20% results in an average concentration that is 17.6% higher. Furthermore, at equal quantity of adherent mortar, an increase of 100% in the diffusivity of said adherent mortar leads to a 23% increase in average concentration. Ultimately, it appears that the percentage of diffusive surface has a greater impact on the overall concrete response than the diffusive properties of the adherent mortar.

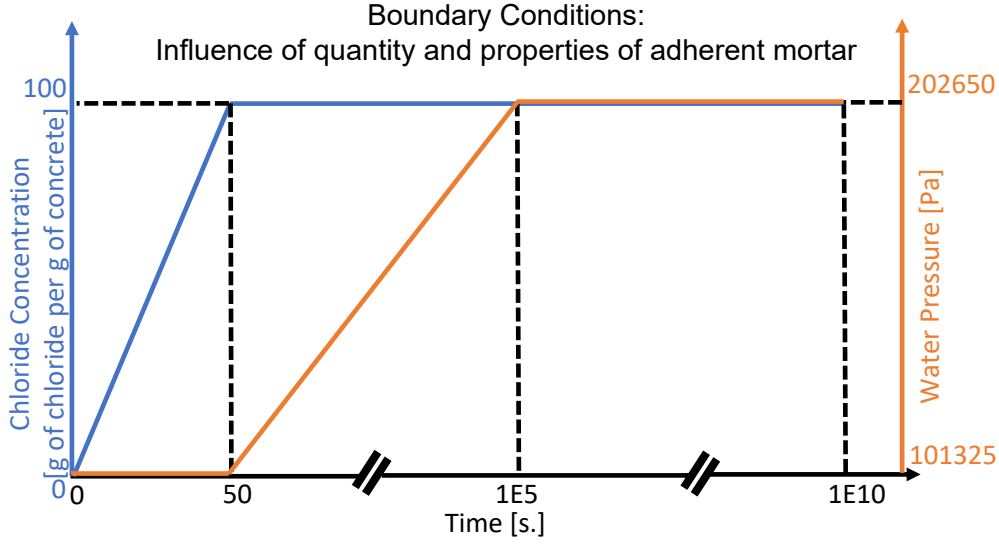


Figure 22: Boundary Conditions for the sensitivity analysis on the influence of the quantity and properties of the adherent mortar inside the RVE. The BC are applied on the left border of the macroscale mesh: water pressure and chloride concentration.

5. Conclusion

In this paper, a multiscale multiphysics model has been described, developed and validated. Subsequently, this model was utilised to replicate an experiment and furthermore, to achieve a real life scenario. Based on the numerical results, it has been demonstrated that concrete produced from recycled concrete aggregates is not necessarily less durable when compared to that produced from natural aggregates. Indeed, the non-linearity of the water retention curve and the decrease in relative permeability induced by desaturation balance the results of the two concretes. The Natural Aggregate Concrete therefore tends to allow chloride ions to reach greater depths, but at a lower concentration than the Recycled Aggregate Concrete. However, the adherent mortar in the recycled aggregates possessed identical properties to the parent mortar, although it is commonly described as having more permeable and porous characteristics in the literature, which should be investigated.

A sensitivity study conducted on the RVE revealed that the quantity of adherent mortar

is more important than its intrinsic properties. In fact, increasing the amount of adherent mortar by 20% increased the total chloride concentration by 17.6%, whereas increasing the diffusion coefficient of this mortar by 100% only increased the total chloride concentration by 23%. It is promising as the quantity of adherent mortar is more easily assessed and controlled than its properties.

To increase the confidence in our results, another sensitivity analysis on the RVE should be performed while computing the response on the lock of the application, as well as a sensitivity analysis on the parameters of the water retention curve.

Acknowledgements

Funding: This work is supported by the Wallonia regional government (Belgium) in the framework of a FRIA (Fund for Industrial and Agricultural Research) grant.

Competing Interests

The authors declare that they have no known competing financial interests or personal relationships that could have appeared to influence the work reported in this paper.

References

- [1] A. Akbarnezhad, K. C. G. Ong., C. T. Tam, M. H. Zhang, Effects of the Parent Concrete Properties and Crushing Procedure on the Properties of Coarse Recycled Concrete Aggregates, *Journal of Materials in Civil Engineering* 25 (2013) 1795–1802.
- [2] P. Belin, G. Habert, M. Thiery, N. Roussel, Cement paste content and water absorption of recycled concrete coarse aggregates, *Materials and Structures* 47 (2014) 1451–1465.
- [3] D. Pedro, J. de Brito, L. Evangelista, Performance of concrete made with aggregates recycled from precasting industry waste: influence of the crushing process, *Materials and Structures* 48 (2015) 3965–3978.
- [4] Z. Hu, L. Mao, J. Xia, J. Liu, J. Gao, J. Yang, Q. Liu, Five-phase modelling for effective diffusion coefficient of chlorides in recycled concrete, *Magazine of Concrete Research* 70 (2018) 583–594.
- [5] A. Rao, K. N. Jha, S. Misra, Use of aggregates from recycled construction and demolition waste in concrete, *Resources, Conservation and Recycling* 50 (2007) 71–87.

- [6] C. Sun, Q. Chen, J. Xiao, W. Liu, Utilization of waste concrete recycling materials in self-compacting concrete, *Resources, Conservation & Recycling* 161 (2020) 104930.
- [7] G. Fathifazl, A. G. Razaqpur, O. B. Isgor, A. Abbas, B. Fournier, S. Foo, Creep and drying shrinkage characteristics of concrete produced with coarse recycled concrete aggregate, *Cement and Concrete Composites* 33 (2011) 1026–1037.
- [8] P. S. Lovato, E. Possan, D. C. C. D. Molin, Â. B. Masuero, J. L. D. Ribeiro, Modeling of mechanical properties and durability of recycled aggregate concretes, *Construction and Building Materials* 26 (2012) 437–447.
- [9] N. Biglarijoo, M. Nili, S. M. Hosseini, M. Razmara, S. Ahmadi, P. Razmara, Modelling and optimisation of concrete containing recycled concrete aggregate and waste glass, *Magazine of Concrete Research* 69 (2017) 306–316.
- [10] Z. Zhao, L. Courard, F. Michel, S. Delvoie, M. E. Bouarroudj, C. Colman, Properties of concrete with recycled construction and demolition wastes: a research experience in Belgium, *Industry-Academia Forum on Advances in Structural Engineering*, Tongji University, Shanghai (7-9 September 2018), 2018.
- [11] P. S. Mangat, B. T. Molloy, Prediction of long term chloride concentration in concrete, *Materials and Structures* 27 (1994) 338–346.
- [12] M. Morga, G. C. Marano, Chloride Penetration in Circular Concrete Columns, *International Journal of Concrete Structures and Materials* 9 (2015) 173–183.
- [13] U. Angst, B. Elsener, C. K. Larsen, Ø. Vennesland, Critical chloride content in reinforced concrete - A review, *Cement and Concrete Research* 39 (2009) 1122–1138.
- [14] E. J. Garboczi, D. P. Bentz, Multiscale Analytical/Numerical Theory of the Diffusivity of Concrete, *Advanced Cement Based Materials* 8 (1998) 77–88.
- [15] F. Bertrand, O. Buzzi, P. Bésuelle, F. Collin, Hydro-mechanical modelling of multiphase flow in naturally fractured coalbed using a multiscale approach, *Journal of Natural Gas Science and Engineering* 78 (2020) 103303.
- [16] F. Nilén, F. Larsson, K. Lundgren, K. Runesson, FE² Method for Coupled Transient Diffusion Phenomena in Concrete, *Journal of Engineering Mechanics* 141 (2014) 04014110.
- [17] J. Bear, A. Verruijt, Modeling Groundwater Flow and Pollution, D. Reidel Publishing Company, 1987.
- [18] R. M. Bowen, Incompressible porous media models by use of the theory of mixtures, *International Journal of Engineering Science* 18 (1980) 1129–1148.
- [19] A. Bensoussan, J.-L. Lions, G. Papanicolaou, Asymptotic analysis for periodic structures, volume 5, North-Holland Publishing Company Amsterdam, 1978.
- [20] R. J. M. Smit, W. A. M. Brekelmans, H. E. H. Meijer, Prediction of the mechanical behavior of nonlinear heterogeneous systems by multi-level finite element modeling, *Computer Methods in Applied*

Mechanics and Engineering 155 (1998) 181–192.

- [21] V. Kouznetsova, W. A. M. Brekelmans, F. P. T. Baaijens, An approach to micro-macro modeling of heterogeneous materials, *Computational Mechanics* 27 (2001) 37–48.
- [22] J. Desrues, A. Argilaga, D. Caillerie, G. Combe, T. K. Nguyen, V. Richefeu, S. Dal Pont, From discrete to continuum modelling of boundary value problems in geomechanics: An integrated fem-dem approach, *International Journal for Numerical and Analytical Methods in Geomechanics* 43 (2019) 919–955.
- [23] A. Fanara, L. Courard, F. Collin, Numerical and experimental study of chloride ion transport in recycled aggregates concrete, *Academic Journal of Civil Engineering, Special Issue - NoMaD 2022* 40 (2023).
- [24] A. Fanara, L. Courard, F. Collin, FE2 multiscale modelling of chloride ions transport in recycled aggregates concrete, in: G. Meschke, B. Pichler, J. G. Rots (Eds.), *Computational Modelling of Concrete and Concrete Structures, volume 1*, Technische Universität Wien, Taylor and Francis Group, 2022, pp. 66–75.
- [25] F. Nilenius, *Moisture and Chloride Transport in Concrete - Mesoscale Modelling and Computational Homogenization*, Ph.D. thesis, Chalmers University of Technology, Gothenburg, Sweden, 2014.
- [26] V. Kouznetsova, M. G. D. Geers, W. A. M. Brekelmans, Multi-scale constitutive modelling of heterogeneous materials with a gradient-enhanced computational homogenization scheme, *International Journal for Numerical Methods in Engineering* 54 (2002) 1235–1260.
- [27] M. T. Van Genuchten, A Closed-form Equation for Predicting the Hydraulic Conductivity of Unsaturated Soils, *Soil Science Society of America Journal* 44 (1980) 892:898.
- [28] A. Fanara, L. Courard, F. Collin, J. Hubert, Transfer properties in recycled aggregates concrete: Experimental and numerical approaches, *Construction and Building Materials* 326 (2022) 126778.
- [29] F. Collin, X. Li, J. Radu, R. Charlier, Thermo-hydro-mechanical coupling in clay barriers, *Engineering Geology* 64 (2002) 179–193.
- [30] M. Nagesh, B. Bhattacharjee, Modeling of Chloride Diffusion in Concrete and Determination of Diffusion Coefficients, *Materials Journal* 95 (1998) 113–120.
- [31] A. Ababneh, F. Benboudjema, Y. Xi, Chloride Penetration in Nonsaturated Concrete, *Journal of Materials in Civil Engineering* 15 (2003) 183–191.
- [32] V. Baroghel-Bouny, M. Thiéry, X. Wang, Modelling of isothermal coupled moisture-ion transport in cementitious materials, *Cement and Concrete Research* 41 (2011) 828–841.
- [33] Q. Liu, D. Easterbrook, J. Yand, L. Li, A three-phase, multi-component ionic transport model for simulation of chloride penetration in concrete, *Engineering Structures* 86 (2015) 122–133.
- [34] L. Wu, W. Li, X. Yu, Time-dependent chloride penetration in concrete in marine environments, *Construction and Building Materials* 152 (2017) 406–413.

- [35] P. Biver, Phenomenal and Numerical study on the propagation of misicible pollutants in a medium with multiple porosity, Ph.D. thesis, University of Liège, 1993.
- [36] F. Marinelli, A. van den Eijnden, Y. Sieffert, R. Chambon, F. Collin, Modeling of granular solids with computational homogenization: Comparison with biot’s theory, *Finite Elements in Analysis and Design* 119 (2016) 45–62.
- [37] Y. Xi, Z. P. Bazant, Modeling Chloride Penetration in Saturated Concrete, *Journal of Materials in Civil Engineering* 11 (1999) 58–65.
- [38] G. Sun, Y. Zhang, W. Sun, Z. Liu, C. Wang, Multi-scale prediction of the effective chloride diffusion coefficient of concrete, *Construction and Building Materials* 25 (2011) 3820–3831.
- [39] J. Ying, L. Shen, J. Xiao, M. A. Bradford, Five-phase composite sphere model for chloride diffusivity prediction of recycled aggregate concrete, *Magazine of Concrete Research* 65 (2013) 573–588.
- [40] L. Jin, H. Yu, T. Fan, T. Dong, P. Jiao, J. Duan, Experimental and computational modeling of chloride transport behavior in fully recycled coarse aggregate concrete, *Construction and Building Materials* 360 (2022) 129592.
- [41] V. Holla, G. Vu, J. J. Timothy, F. Diewald, C. Gehlen, G. Meschke, Computational Generation of Virtual Concrete Mesostructures, *Materials* 14 (2021) 3782.
- [42] C. Geuzaine, J.-F. Remacle, Gmsh: a three-dimensional finite element mesh generator with built-in pre- and post-processing facilities., *International Journal for Numerical Methods in Engineering* 79 (2009) 1309–1331.
- [43] X. Chen, X. Zhang, Z. Wu, Analytical Solution for One-Dimensional Transport of Particles considering Dispersion in Deposition Kinetics, *Hindawi, Geofluids* 2019 (2019) 1941426.
- [44] J. Zuquan, Z. Xia, Z. Tiejun, L. Jianqing, Chloride ions transportation behavior and binding capacity of concrete exposed to different marine corrosion zones, *Construction and Building Materials* 177 (2018) 170–183.

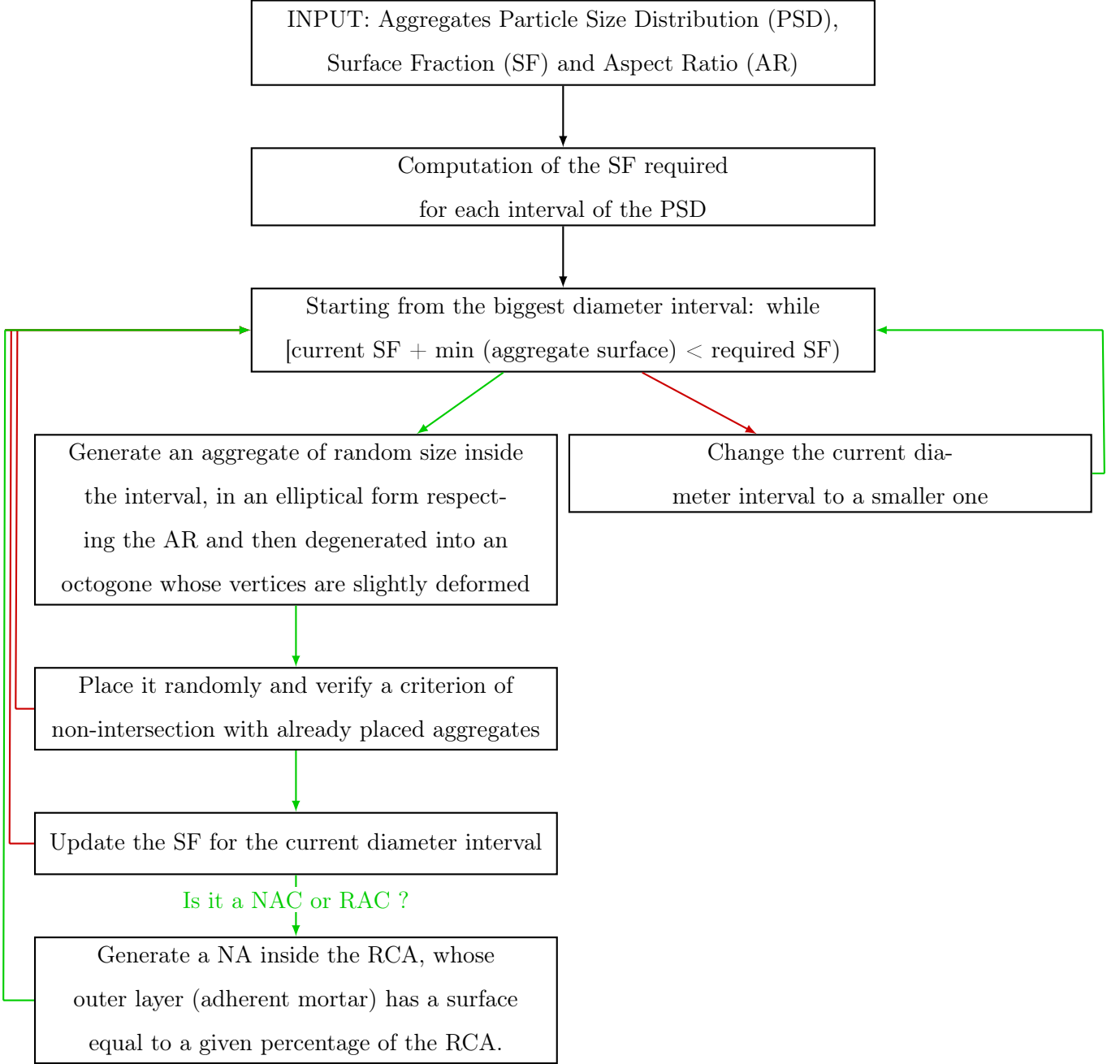


Figure 2: Algorithm generating the RVE. A red arrows means 'No' while a green arrow means 'Yes'.

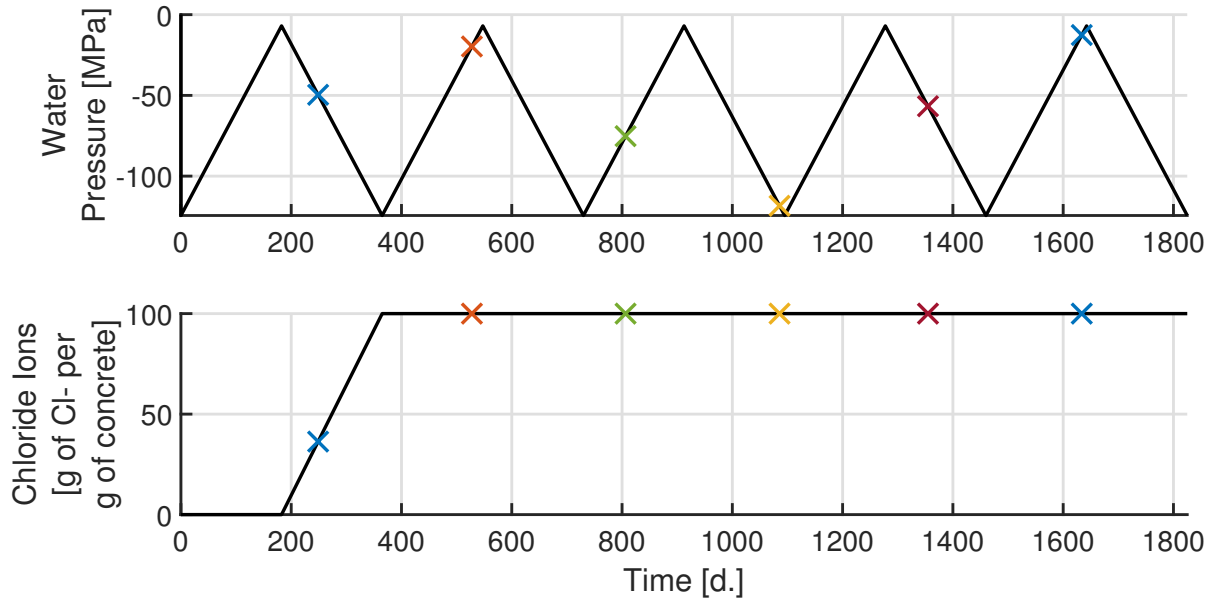


Figure 5: Boundary Conditions of the validation under unsaturated conditions. Each marker corresponds to a time represented in Figures 6 and 7.

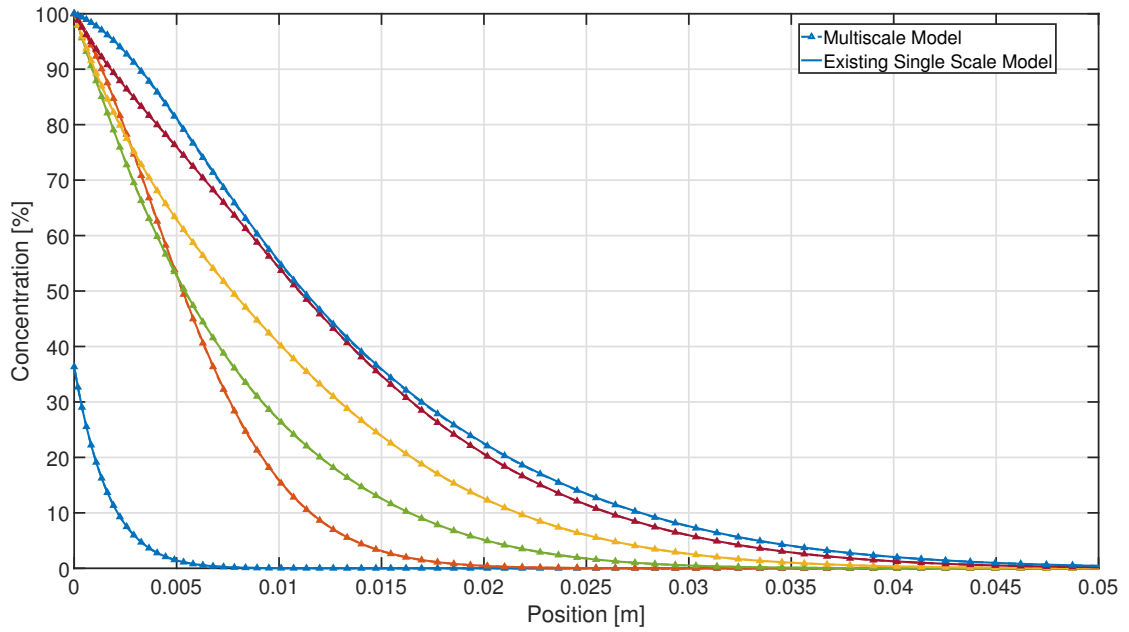


Figure 6: Numerical validation of the multiscale model under unsaturated conditions: results in terms of chloride ions concentration. Each color represents a distinct elapsed time (see Figure 5).

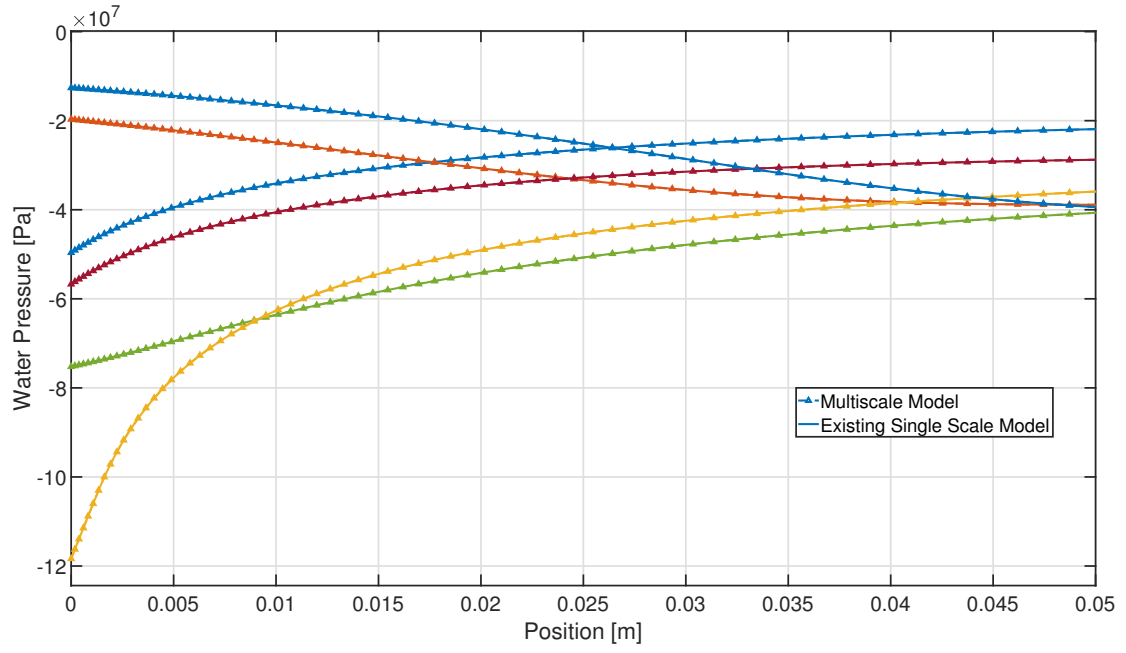


Figure 7: Numerical validation of the multiscale model under unsaturated conditions: results in terms of water pressure. Each color represents a distinct elapsed time (see Figure 5).

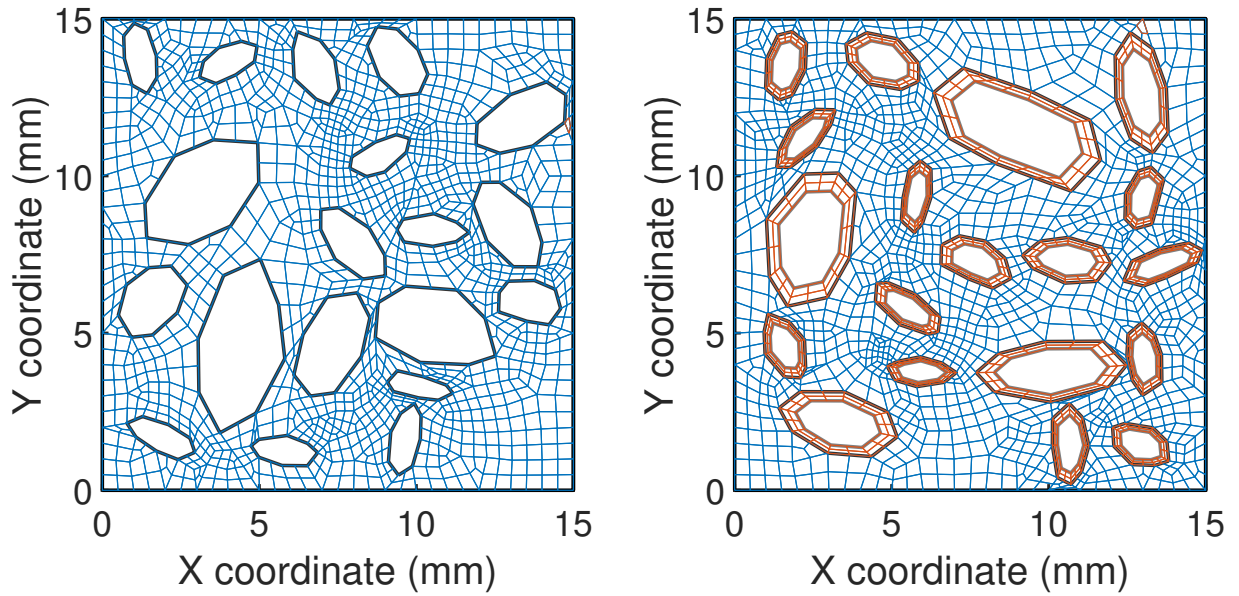


Figure 8: RVE mesh representing the two types of concrete used: NAC (left) and RAC (right).

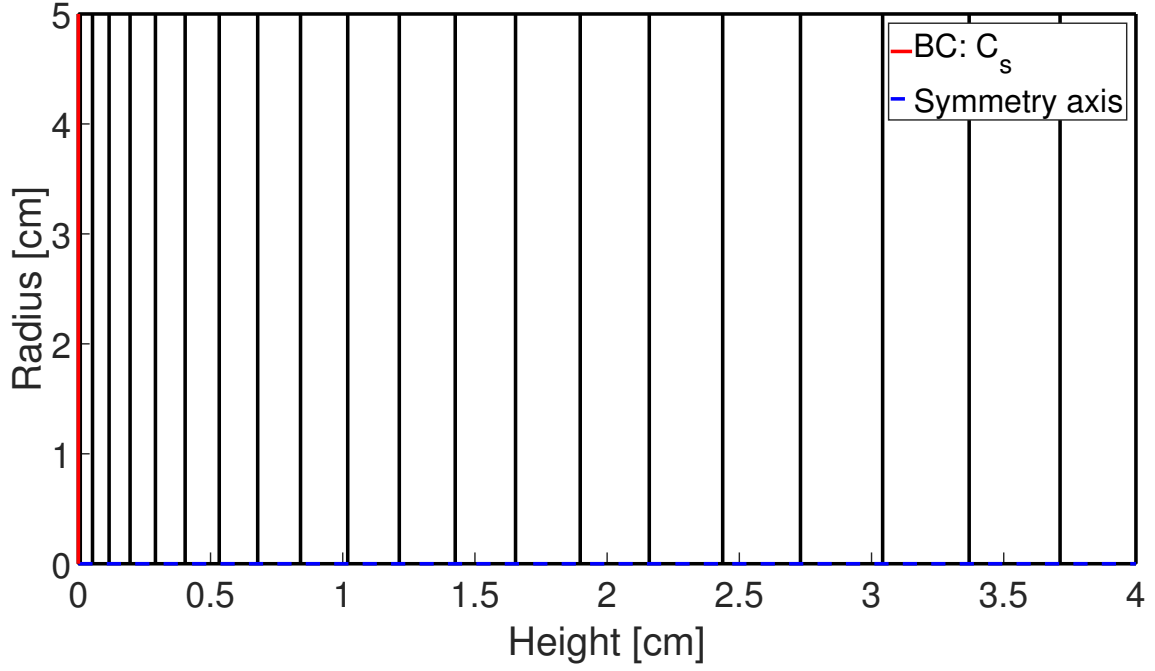


Figure 9: Macroscale mesh representing the experiment performed, with the Boundary Conditions applied according to Table 2. The diameter of the experimental sample is divided by two under axisymmetric conditions.

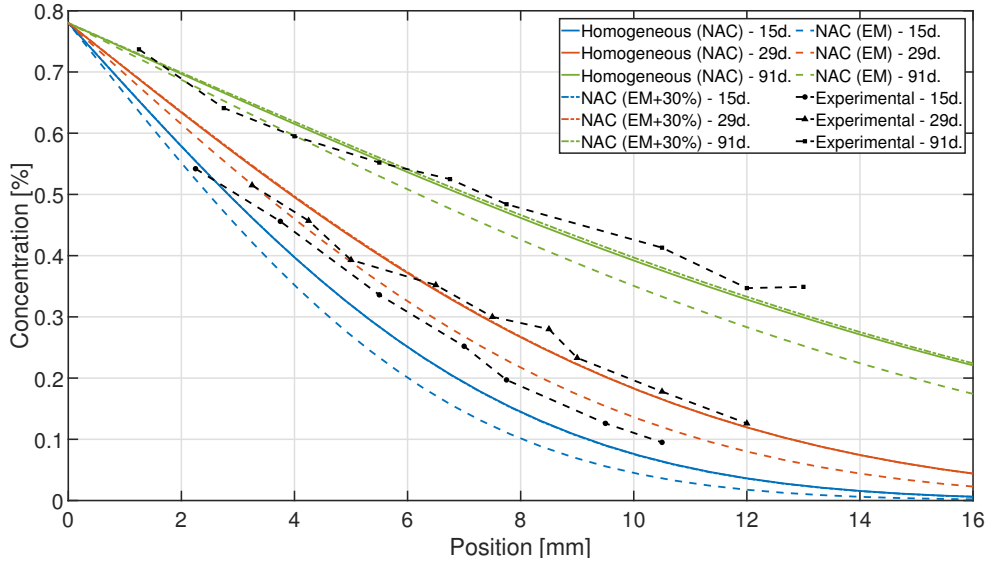


Figure 10: Replication of the experiment of diffusion under unsteady state. The experimental results are compared with the results of our model for a homogeneous RVE with properties of the NAC, or for a RVE representing the NAC with properties of the mortar E-M.

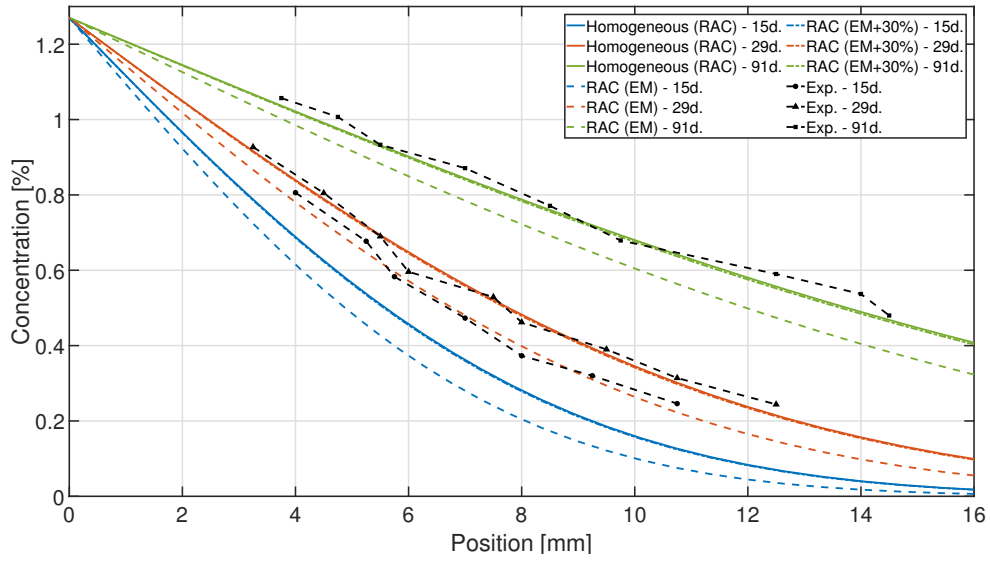


Figure 11: Replication of the experiment of diffusion under unsteady state. The experimental results are compared with the results of our model for a homogeneous RVE with properties of the RAC, or for a RVE representing the RAC with properties of the mortar E-M.

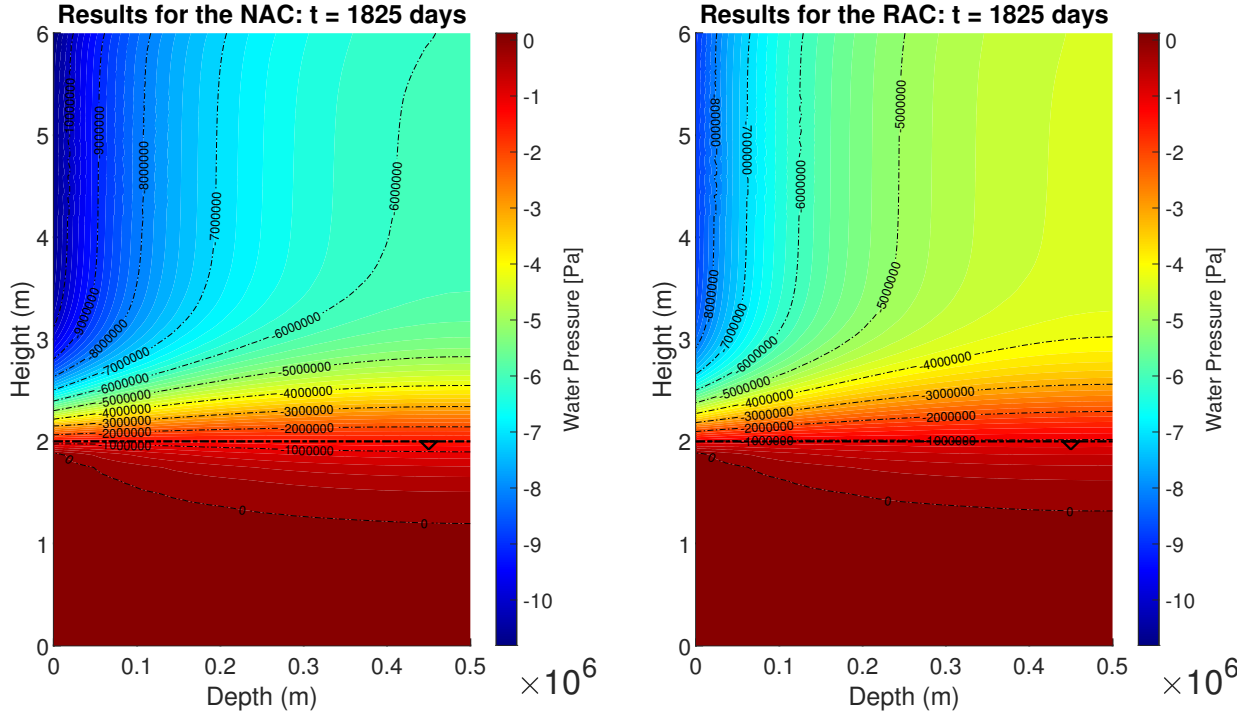


Figure 13: Results of the application: water pressure for the NAC (left) and RAC (right) after 1825 days.

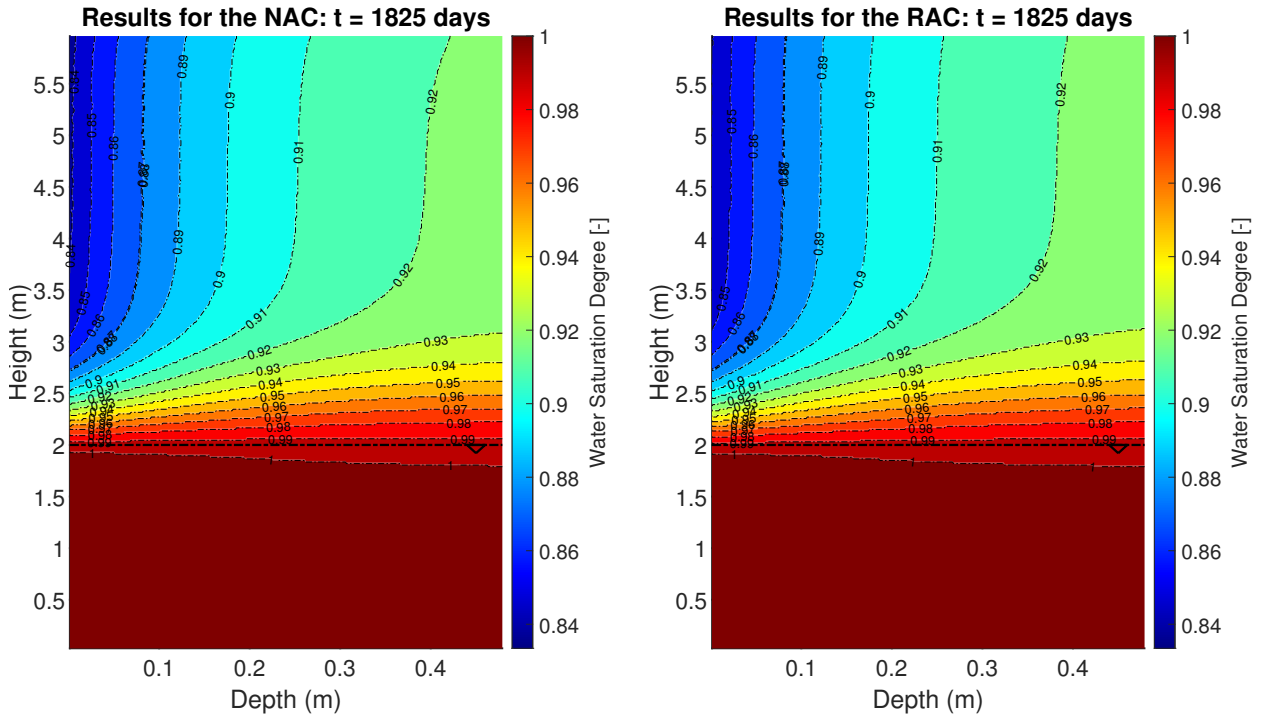


Figure 14: Results of the application: water saturation degree for the NAC (left) and RAC (right) after 1825 days.

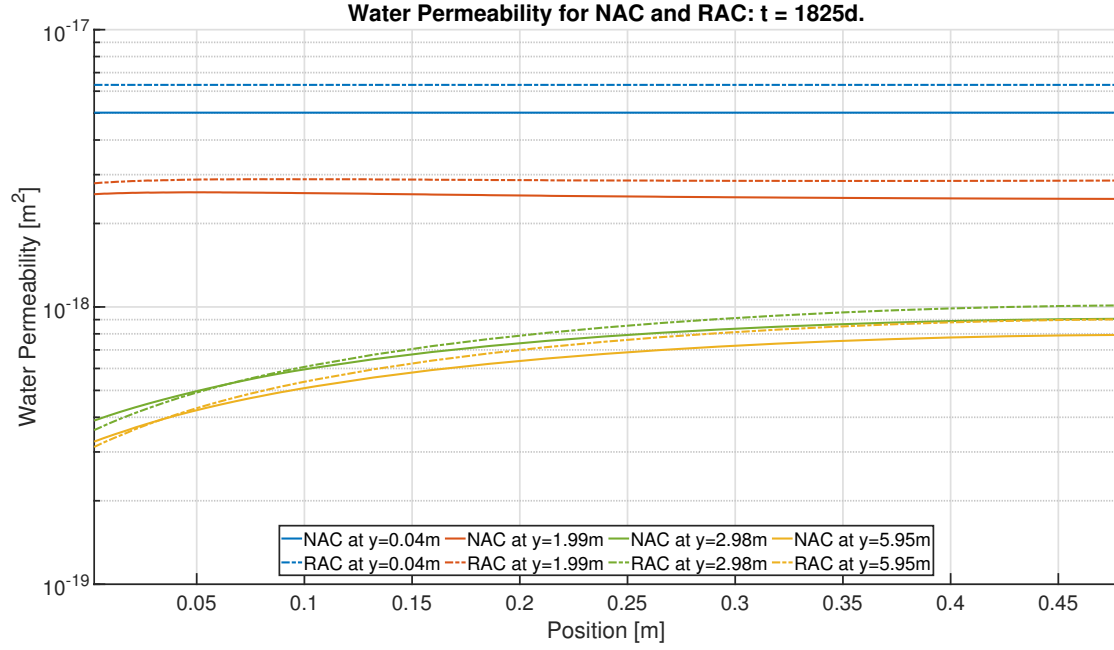


Figure 15: Results of the application: evolution of the water permeability with depth for the NAC and RAC, at different height on the lock wall and at 1825 days.

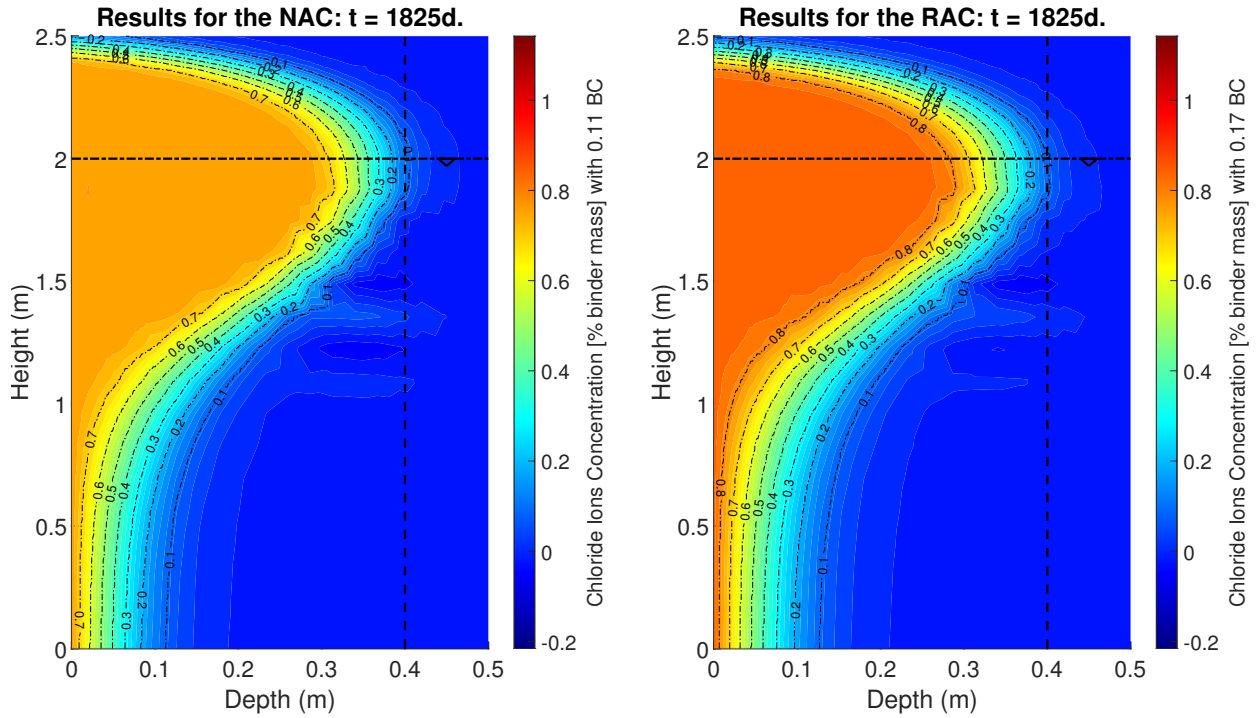


Figure 16: Results of the application: chloride ions concentration for the NAC (left) and RAC (right) after 1825 days, expressed as a percentage of the binder mass.

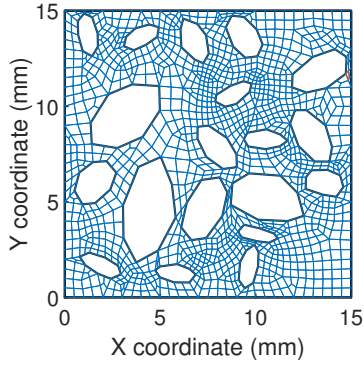


Figure 19: RVE representing the NAC.

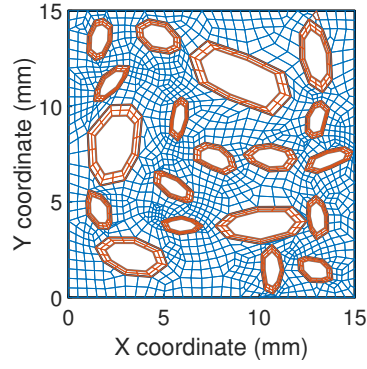


Figure 20: RVE representing the RAC.

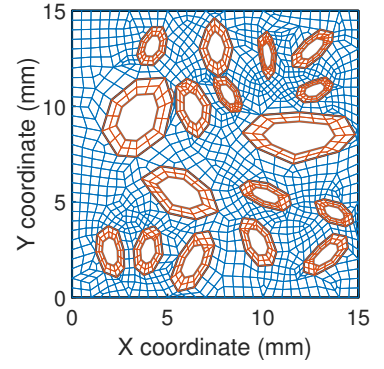


Figure 21: RVE: RAC with 20% more adherent mortar.

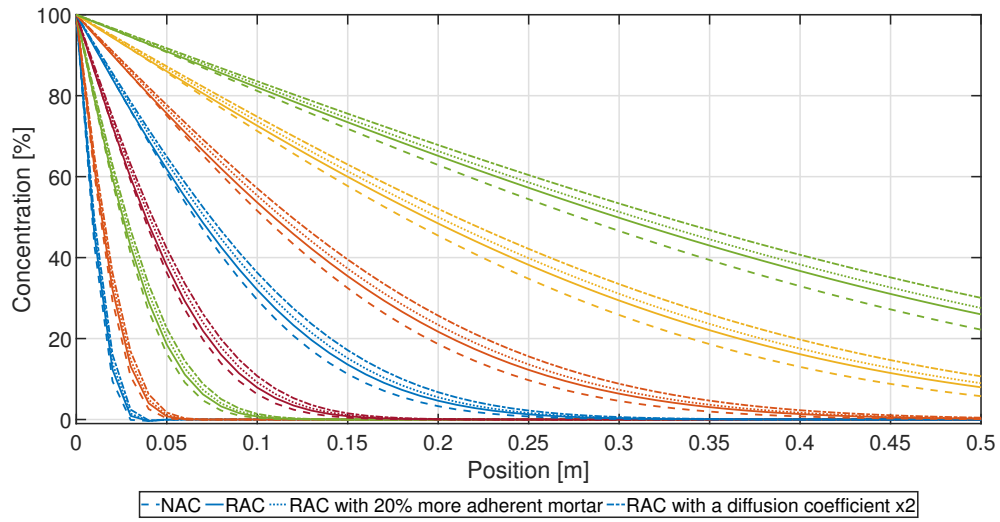


Figure 23: Results of the diffusion of chloride ions inside two different RVEs (NAC and RAC) under increasing water pressure and chloride content at the left border. Each color represents a distinct elapsed time.